INTERNATIONAL JOURNAL FOR NUMERICAL METHODS IN ENGINEERING, VOL. 40, 4611–4632 (1997)

NUMERICAL ANALYSIS OF EDGE SINGULARITIES IN THREE-DIMENSIONAL ELASTICITY

ZOHAR YOSIBASH*

Pearlstone Center for Aeronautical Engineering Studies, Department of Mechanical Engineering, Ben-Gurion University of the Negev, Beer-Sheva 84105, Israel

ABSTRACT

A numerical method is described for the computation of eigenpairs which characterize the exact solution of linear elastostatic problems in three-dimensions in the vicinity of edge singularities. These may be caused by re-entrant corners, abrupt changes in boundary conditions or material properties.

Such singularities are of great interest from the point of view of failure initiation: The eigenpairs characterize the straining modes and their amplitudes quantify the amount of energy residing in particular straining modes. For this reason, failure theories directly or indirectly involve the eigenpairs and their amplitudes.

This paper addresses the problem of determining the edge eigenpairs numerically on the basis of the modified Steklov formulation (presented in Reference 1 in a 2-D framework) in conjunction with the *p*-version of the finite element method. Numerical results are presented for several cases including isotropic as well as anisotropic multi-material interfaces. © 1997 John Wiley & Sons, Ltd.

Int. J. Numer. Meth. Engng., **40**, 4611–4632 (1997)

No. of Figures: 13. No. of Tables: 5. No. of References: 24.

KEY WORDS: three-dimensional elasticity; singularities; finite element methods; *p*-version; Steklov method; failure/fracture analysis; multi-material interfaces; delamination

1. INTRODUCTION

Realistic mechanical response of structural objects undergoing small displacements is governed by the equations of three-dimensional linear elasticity. Many three-dimensional objects have surface boundaries which intersect at curves called edges, and some of these edges intersect at points called vertices. The behaviour of the elastic solution in the neighbourhood of edges has been a subject of intensive research during the past 30 years especially with regard to interface edge cracks and interlaminar stresses in composite laminates. Renewed interest in the solution of the three-dimensional linear elastic problem at edges occurred due to increasing interest in laminated composites and electronic devices. In the vicinity of these edges the stress tensor exhibits singular behaviour, i.e. tends to infinity as the distance from the edge tends to zero. The displacement solution (associated with the singular stress tensor) is uniquely characterized by a sequence of discrete eigenpairs and their coefficients (in the neighbourhood of edges). These are

* Correspondence to: Zohar Yosibash, Ben-Gurion University of the Negev, Mechanical Engineering Department, P.O. Box 653, Beer-Sheva 84105, Israel

CCC 0029–5981/97/244611–22$17.50

Received 24 November 1996
Revised 27 April 1997

of great interest in structural mechanics because they provide a basis for predicting failure events in the vicinity of edges.

Due to the complex treatment of three-dimensional edge eigenpairs, most of the research on singular stress fields has focused on two-dimensional domains under the assumption of plane stress or plane strain. The reader is referred to the list of publications[1–14] (not exhaustive by any means), and the references therein which address the analytical as well as numerical computation of eigen-pairs in two-dimensions.

The fully three-dimensional edge singularities have been less investigated, especially when associated with anisotropic materials and multi-material interfaces. Analytical methods as in Reference 15 provide the means for computing the eigenpairs for a two-material interface, however, requires extensive mathematics. Several numerical methods, mainly based on the *h*-version of the finite element method have been suggested lately. Among them are Reference 12 in which an excellent reference list to the subject is provided, and Reference 16. These methods provide good results, however, they require the solution of a quadratic eigenproblem (which is an expensive task), do not provide an easy adaptive scheme for assuring the convergence of the computed values, and in Reference 16 the method presented does not provide information on the performance for cases where complex eigenpairs appear. It is felt that the methods in References 12 and 16 fail to indicate these cases which give rise to logarithmic stress singularities.

Herein a numerical procedure based on the *modified Steklov method*, presented in Reference 1 in a two-dimensional setting, is developed. This method computes efficiently and reliably approximations for the edge singular solutions when used in conjunction with the *p*-version of the finite element method. It is general, that is, applicable to edge singularities associated with corners, non-isotropic multi-material interfaces and abrupt changes in boundary conditions.

In Section 2, an explicit formulation of the modified Steklov method for edge singularities is presented. Numerical treatment of the weak modified Steklov formulation by the *p*-version of the finite element method is presented in Section 3. In Section 4, numerical examples are provided. These include edge crack singularities in isotropic and at a bi-material interface, and free edge effects in a two cross-ply anisotropic laminate. The obtained eigenpairs are compared to the exact values, demonstrating the efficiency, accuracy and robustness of the method. We conclude with a summary in Section 5.

2. FORMULATING THE MODIFIED STEKLOV EIGEN-PROBLEM

The elastostatic displacements field in three dimensions, in the vicinity of an edge (which is sufficiently away from a vertex) can be decomposed in terms of edge eigenpairs and edge stress intensity functions (ESIFs). Mathematical details on the decomposition can be found e.g. in References 17–20 and the references therein. A representative three-dimensional domain denoted by Ω, which contains typical 3-D singularities is shown in Figure 1. Edge singularities arise in the neighbourhood of the edges Λ_{ij}, vertex singularities arise in the neighbourhood of vertices A_i, and vertex-edge singularities arise close to vertex/edge intersections. Herein, only edge singularities are treated, whereas the vertex singularities, which are also of major engineering importance, will be addressed in a future work. It shall be assumed that curved edges which intersect at vertices do not exist, and that crack faces, if any, lie in a flat plane.

The edges Λ_{ij}, connecting the vertices, A_i and A_j, are examined. Moving away from the vertex a distance $\delta/2$ ($\delta > 0$), and creating a cylindrical domain of radius $r = R$ having the edge Λ_{ij} as its axis, we define a sub-domain in the vicinity of the edge denoted by $\mathscr{E}_{\delta,R}(\Lambda_{ij})$. Figure 2 shows the

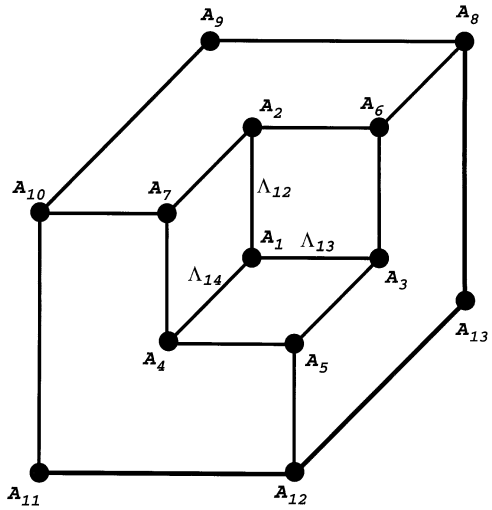

Figure 1. Typical 3-D singularities

edge singularity sub-domain $\mathscr{E}_{\delta,R}(\Lambda_{12})$. The displacements in $\mathscr{E}_{\delta,R}$ can be decomposed as follows:

$$\mathbf{u}(r,\theta,z)=\sum_{k=1}^{K}\sum_{s=0}^{S}a_{ks}(z)r^{\alpha_k}(\ln r)^s\mathbf{f}_{ks}(\theta)+\mathbf{w}(r,\theta,z) \tag{1}$$

where $S\geqslant 0$ is an integer which is zero for most practical problems, except for special cases, $\alpha_{k+1}\geqslant\alpha_k$ are called edge eigenvalues, $a_{ks}(z)$ are analytic in z called ESIFs, and can become very large as they approach one of the vertices, and $\mathbf{f}_{ks}(\theta)$ are analytic in θ, called eigenfunctions. The vector function $\mathbf{w}(r,\theta,z)$ belongs to the Sobolev space $[H^q(\mathscr{E})]^3$, where q depends on K, and can be made as high as required providing that K is large enough. We shall assume that $S=0$, therefore, (1) becomes

$$\mathbf{u}(r,\theta,z)=\sum_{k=1}^{K}a_k(z)r^{\alpha_k}\mathbf{f}_k(\theta)+\mathbf{w}(r,\theta,z) \tag{2}$$

$\mathbf{u}=(u_x\ u_y\ u_z)^{\mathrm{T}}$ is the displacement vector, with $u_x(r,\theta,z)$, $u_y(r,\theta,z)$ and $u_z(r,\theta,z)$ being its components in the x, y and z directions, respectively. We denote the tractions on the boundaries by $\mathbf{T}=(T_x\ T_y\ T_z)^{\mathrm{T}}$ and the Cartesian stress tensor by $\underset{\approx}{\boldsymbol{\sigma}}$, and in vector form by $\boldsymbol{\sigma}=(\sigma_x\ \sigma_y\ \sigma_z\ \tau_{xy}\ \tau_{yz}\ \tau_{xz})^{\mathrm{T}}$. In the vicinity of the edge we assume that no body forces are present.

A sub-domain of $\mathscr{E}_{\delta,R}$ is considered, which is bounded by the surfaces $z=0$ and $z=\Delta$, and by the radii $r=R^*$ and $r=R$. This domain, denoted by Ω_R^*, is shown in Figure 3.

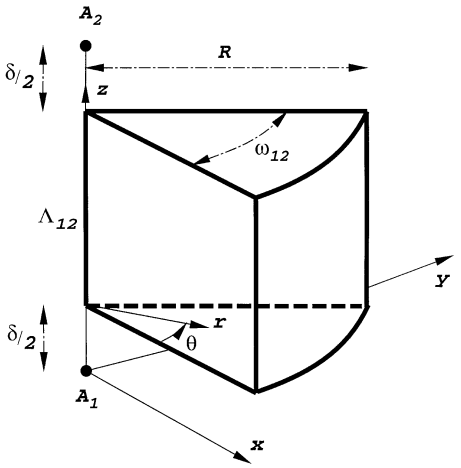

Figure 2. The edge neighborhood $\mathscr{E}_{\delta,R}(\Lambda_{12})$

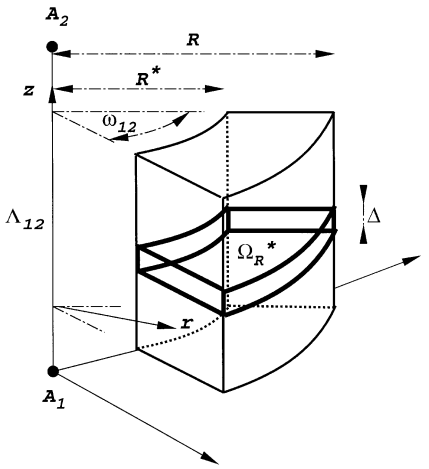

Figure 3. The modified Steklov domain Ω_R^*

The elastostatic problem in 3-D can be cast in terms of stresses over the domain Ω_R^*:

$$\left.\begin{aligned}\partial_x\sigma_x+\partial_y\tau_{xy}+\partial_z\tau_{xz}=0\\ \partial_x\tau_{xy}+\partial_y\sigma_y+\partial_z\tau_{yz}=0\\ \partial_x\tau_{xz}+\partial_y\tau_{yz}+\partial_z\sigma_z=0\end{aligned}\right\}\quad \text{in } \Omega_R^*,\quad \text{where}\quad \begin{aligned}\partial_x &\overset{\text{def}}{=} \frac{\partial}{\partial x}\\ \partial_y &\overset{\text{def}}{=} \frac{\partial}{\partial y}\\ \partial_z &\overset{\text{def}}{=} \frac{\partial}{\partial z}\end{aligned} \tag{3}$$

while on the boundaries of $\theta = 0$ and $\theta = \omega_{ij}$ homogeneous traction boundary conditions are assumed ($\mathbf{T} = \mathbf{0}$). This assumption is only for simplifying the presentation, and the presented methods are equally applicable to homogeneous displacements as well as homogeneous mixed boundary conditions. Boundary conditions on the other four surface areas are yet to be specified.

The stress–displacements relationship through the constitutive material law (Hooke's law) is given by

$$\boldsymbol{\sigma} = [E][D]\mathbf{u} \tag{4}$$

where $[D]$ is the differential operator:

$$[D] \stackrel{\text{def}}{=} \begin{bmatrix} \partial_x & 0 & 0 \\ 0 & \partial_y & 0 \\ 0 & 0 & \partial_z \\ \partial_y & \partial_x & 0 \\ 0 & \partial_z & \partial_y \\ \partial_z & 0 & \partial_x \end{bmatrix} = \underbrace{\begin{bmatrix} \cos\theta & 0 & 0 \\ 0 & \sin\theta & 0 \\ 0 & 0 & 0 \\ \sin\theta & \cos\theta & 0 \\ 0 & 0 & \sin\theta \\ 0 & 0 & \cos\theta \end{bmatrix}}_{[A_r]} \partial_r + \underbrace{\begin{bmatrix} -\sin\theta & 0 & 0 \\ 0 & \cos\theta & 0 \\ 0 & 0 & 0 \\ \cos\theta & -\sin\theta & 0 \\ 0 & 0 & \cos\theta \\ 0 & 0 & -\sin\theta \end{bmatrix}}_{[A_\theta]} \frac{\partial_\theta}{r}$$
$$+ \underbrace{\begin{bmatrix} 0 & 0 & 0 \\ 0 & 0 & 0 \\ 0 & 0 & 1 \\ 0 & 0 & 0 \\ 0 & 1 & 0 \\ 1 & 0 & 0 \end{bmatrix}}_{[A_z]} \partial_z \tag{5}$$

and $[E]$ is the 6×6 symmetric material matrix which is given for an isotropic material by

$$[E] = \frac{E}{(1+\nu)(1-2\nu)} \begin{bmatrix} (1-\nu) & \nu & \nu & 0 & 0 & 0 \\ & (1-\nu) & \nu & 0 & 0 & 0 \\ & & (1-\nu) & 0 & 0 & 0 \\ & & & (1-2\nu)/2 & 0 & 0 \\ & & & & (1-2\nu)/2 & 0 \\ & & & & & (1-2\nu)/2 \end{bmatrix}$$

where E is Young's modulus and ν is the Poisson ratio.

Multiplying (3) by $\mathbf{v}^{\mathrm{T}} = (v_x\, v_y\, v_z) \in [H^1(\Omega_R^*)]^3$, integrating over the domain Ω_R^* shown in Figure 3, then using Green's theorem, and following the steps presented in Reference 21, Chapter 13, one obtains the weak form for the elastostatic problem:

$$\begin{gathered} \text{Seek } \mathbf{u} \in [H^1(\Omega_R^*)]^3 \quad \text{such that} \\ \mathscr{B}(\mathbf{u}, \mathbf{v}) = \mathscr{F}(\mathbf{v}), \quad \forall \mathbf{v} \in [H^1(\Omega_R^*)]^3 \end{gathered} \tag{6}$$

where

$$\mathscr{B}(\mathbf{u},\mathbf{v}) \overset{\text{def}}{=} \int_0^{\Delta}\int_R^{R^*}\int_0^{\omega_{12}} ([D]\mathbf{v})^{\mathrm{T}}[E][D]\mathbf{u}r\,\mathrm{d}\theta\,\mathrm{d}r\,\mathrm{d}z \tag{7}$$

$$\mathscr{F}(\mathbf{v}) \overset{\text{def}}{=} \int\int_{\partial\Omega_R^*} (\mathbf{v})^{\mathrm{T}}\,\mathbf{T}\,\mathrm{d}A \tag{8}$$

If homogeneous displacement boundary conditions are prescribed on the faces $\theta = 0, \omega_{12}$, then the weak form (6) remains unchanged except for the spaces in which $\mathbf{u}$ and $\mathbf{v}$ lie.

2.1. Notations and mathematical relationships

Some new notations and mathematical relationships are derived to simplify the manipulations required for deriving the modified Steklov eigenformulation. In view of (2), we seek for functions $\mathbf{u}$ in Ω_{R^*} (respectively, $\mathbf{v}$) which can be represented by pairs of α and $\mathbf{f}(\theta)$ as follows:

$$\mathbf{u} \overset{\text{def}}{=} A(z)r^{\alpha}\begin{Bmatrix} f_x(\theta) \\ f_y(\theta) \\ f_z(\theta) \end{Bmatrix} = A(z)r^{\alpha}\mathbf{f}(\theta), \quad \mathbf{v} \overset{\text{def}}{=} B(z)r^{\alpha}\mathbf{f}(\theta) \tag{9}$$

We also denote the *in-plane* variation of the displacements as follows:

$$\tilde{\mathbf{u}}(r,\theta) \overset{\text{def}}{=} \mathbf{u}/A(z) \quad \tilde{\mathbf{v}}(r,\theta) \overset{\text{def}}{=} \mathbf{v}/B(z) \tag{10}$$

Applying (5)–(9) one obtains

$$[D]\mathbf{u} = \frac{A(z)}{r}(\alpha[A_r] + [A_\theta]\partial_\theta)r^{\alpha}\mathbf{f} + A'(z)[A_z]r^{\alpha}\mathbf{f} \tag{11}$$

The relationship between tractions and the stress on a face having an outer normal vector n is given by

$$\mathbf{T} = \underset{\approx}{\boldsymbol{\sigma}}\mathbf{n} = \underbrace{\begin{bmatrix} n_x & 0 & 0 & n_y & 0 & n_z \\ 0 & n_y & 0 & n_x & n_z & 0 \\ 0 & 0 & n_z & 0 & n_y & n_x \end{bmatrix}}_{[n]}\boldsymbol{\sigma} \tag{12}$$

Using (11) and (4) in conjunction with (12) one obtains

$$\mathbf{T} = r^{\alpha}[n][E]\left\{\frac{A(z)}{r}(\alpha[A_r]\mathbf{f} + [A_\theta]\mathbf{f}') + A'(z)[A_z]\mathbf{f}\right\} \tag{13}$$

The relationship (13) can also be stated in terms of $\tilde{\mathbf{u}}$:

$$\mathbf{T} = [n][E]\left\{\frac{A(z)}{r}(\alpha[A_r]\tilde{\mathbf{u}} + [A_\theta]\partial_\theta\tilde{\mathbf{u}}) + A'(z)[A_z]\tilde{\mathbf{u}}\right\} \tag{14}$$

2.2. Modified Steklov eigenformulation

The right-hand side in (6) is being considered. $\mathscr{F}(\mathbf{v})$ is split into three parts; the first part, $\mathscr{F}_1$, is defined on the two straight faces of Ω_{R^*}, $z=0$ where $\mathbf{n}^{\mathrm{T}}=(0\ 0\ -1)$, and $z=\Delta$ where $\mathbf{n}^{\mathrm{T}}=(0\ 0\ 1)$:

$$\mathscr{F}_1(v)=\int_{R^*}^{R}\int_0^{\omega_{12}}\left\{(B(z)r^{\alpha}\mathbf{f}^{\mathrm{T}})r^{\alpha}[n][E]\left[\frac{A(z)}{r}(\alpha[A_r]\mathbf{f}+[A_\theta]\mathbf{f}')+A'(z)[A_z]\mathbf{f}\right]\right|_{z=\Delta}$$

$$+(B(z)r^{\alpha}\mathbf{f}^{\mathrm{T}})r^{\alpha}[n][E]\left[\frac{A(z)}{r}(\alpha[A_r]\mathbf{f}+[A_\theta]\mathbf{f}')+A'(z)[A_z]\mathbf{f}\right]\Bigg|_{z=0}\Bigg\}r\,\mathrm{d}r\,\mathrm{d}\theta.$$

Notice that on the face $z=0$, $[n]=-[A_z]^{\mathrm{T}}$, and on the face $z=\Delta$, $[n]=[A_z]^{\mathrm{T}}$, then $\mathscr{F}_1$ becomes

$$\mathscr{F}_1(\mathbf{v})=A(z)B(z)\left|_{z=0}^{z=\Delta}\frac{r^{2\alpha+1}}{2\alpha+1}\right|_{r=R^*}^{r=R}\int_0^{\omega_{12}}\mathbf{f}^{\mathrm{T}}[A_z]^{\mathrm{T}}[E](\alpha[A_r]\mathbf{f}+[A_\theta]\mathbf{f}')\,\mathrm{d}\theta \tag{15}$$

$$+A'(z)B(z)\left|_{z=0}^{z=\Delta}\frac{r^{2\alpha+2}}{2\alpha+2}\right|_{r=R^*}^{r=R}\int_0^{\omega_{12}}\mathbf{f}^{\mathrm{T}}[A_z]^{\mathrm{T}}[E][A_z]\mathbf{f}\,\mathrm{d}\theta \tag{16}$$

The second part, $\mathscr{F}_2$, is defined on the two cylindrical faces of Ω_{R^*}, $r=R$ where $\mathbf{n}^{\mathrm{T}}=(\cos\theta\ \sin\theta\ 0)$, and $r=R^*$ where $\mathbf{n}^{\mathrm{T}}=-(\cos\theta\ \sin\theta\ 0)$:

$$\mathscr{F}_2(\mathbf{v})=\int_0^{\Delta}\int_0^{\omega_{12}}B(z)\tilde{\mathbf{v}}^{\mathrm{T}}[n][E]\left\{\frac{A(z)}{r}(\alpha[A_r]\tilde{\mathbf{u}}+[A_\theta]\partial_\theta\tilde{\mathbf{u}})+A'(z)[A_z]\tilde{\mathbf{u}}\right\}r\Big|_{r=R}$$

$$+B(z)\tilde{\mathbf{v}}^{\mathrm{T}}[n][E]\left\{\frac{A(z)}{r}(\alpha[A_r]\tilde{\mathbf{u}}+[A_\theta]\partial_\theta\tilde{\mathbf{u}})+A'(z)[A_z]\tilde{\mathbf{u}}\right\}r\Big|_{r=R^*}\mathrm{d}z\,\mathrm{d}\theta$$

On the cylindrical face $r=R^*$, $[n]=-[A_r]^{\mathrm{T}}$, and on the face $r=R$, $[n]=[A_r]^{\mathrm{T}}$, then $\mathscr{F}_2(\mathbf{v})$ becomes

$$\mathscr{F}_2(\mathbf{v})=\left(\int_0^{\Delta}A(z)B(z)\,\mathrm{d}z\right)\left\{\alpha\int_0^{\omega_{12}}\tilde{\mathbf{v}}^{\mathrm{T}}[A_r]^{\mathrm{T}}[E]\,[A_r]\tilde{\mathbf{u}}\Big|_{r=R^*}^{r=R}\mathrm{d}\theta\right. \tag{17}$$

$$\left.+\int_0^{\omega_{12}}\tilde{\mathbf{v}}^{\mathrm{T}}[A_r]^{\mathrm{T}}[E][A_\theta]\partial_\theta\tilde{\mathbf{u}}\Big|_{r=R^*}^{r=R}\mathrm{d}\theta\right\} \tag{18}$$

$$+\int_0^{\Delta}A'(z)B(z)\,\mathrm{d}z\int_0^{\omega_{12}}r\tilde{\mathbf{v}}^{\mathrm{T}}[A_r]^{\mathrm{T}}[E][A_z]\tilde{\mathbf{u}}\Big|_{r=R^*}^{r=R}\mathrm{d}\theta \tag{19}$$

The third part of the linear form $\mathscr{F}$, defined of the straight faces $\theta=0$ and $\theta=\omega_{12}$, vanishes. This is because we assume $\mathbf{T}=\mathbf{0}$ on these faces.

The bi-linear form in (6) is being considered. Substitute (11) into (7), we may split $\mathscr{B}(\mathbf{u}, \mathbf{v})$ into three parts $\mathscr{B} \overset{\text{def}}{=} \mathscr{B}_1 + \mathscr{B}_2 + \mathscr{B}_3$, given by

$$\mathscr{B}_1 = \left(\int_0^{\Delta} A(z)B(z)\,\mathrm{d}z \right) \int_{R^*}^{R} \int_0^{\omega_{12}} \left\{ \left([A_r]\partial_r + [A_\theta]\frac{\partial_\theta}{r} \right) \tilde{\mathbf{v}} \right\}^{\mathrm{T}} [E] \left\{ \left([A_r]\partial_r + [A_\theta]\frac{\partial_\theta}{r} \right) \tilde{\mathbf{u}} \right\} r\,\mathrm{d}r\,\mathrm{d}\theta \tag{20}$$

$$\mathscr{B}_2 = \left(\int_0^{\Delta} A(z)B'(z)\,\mathrm{d}z \right) \frac{r^{2\alpha+1}}{2\alpha+1} \Bigg|_{r=R^*}^{r=R} \int_0^{\omega_{12}} \mathbf{f}^{\mathrm{T}}[A_z]^{\mathrm{T}}[E](\alpha[A_r]\mathbf{f} + [A_\theta]\mathbf{f}')\,\mathrm{d}\theta$$
$$+ \left(\int_0^{\Delta} A'(z)B(z)\,\mathrm{d}z \right) \frac{r^{2\alpha+1}}{2\alpha+1} \Bigg|_{r=R^*}^{r=R} \int_0^{\omega_{12}} (\mathbf{f}^{\mathrm{T}}\alpha[A_r]^{\mathrm{T}} + \mathbf{f}'^{\mathrm{T}}[A_\theta]^{\mathrm{T}})[E][A_z]\mathbf{f}\,\mathrm{d}\theta \tag{21}$$

$$\mathscr{B}_3 = \left(\int_0^{\Delta} A'(z)B'(z)\,\mathrm{d}z \right) \int_{R^*}^{R} \int_0^{\omega_{12}} \tilde{\mathbf{v}}^{\mathrm{T}}[A_z]^{\mathrm{T}}[E][A_z]\tilde{\mathbf{u}}\,r\,\mathrm{d}r\,\mathrm{d}\theta \tag{22}$$

Examining the bi-linear form $\mathscr{B}_2$ it can be shown that for any material matrix,

$$\mathbf{f}^{\mathrm{T}}[A_z]^{\mathrm{T}}[E](\alpha[A_r]\,\mathbf{f} + [A_\theta]\mathbf{f}') = (\mathbf{f}^{\mathrm{T}}\alpha[A_r]^{\mathrm{T}} + \mathbf{f}'^{\mathrm{T}}[A_\theta]^{\mathrm{T}})\,[E][A_z]\mathbf{f} \tag{23}$$

and integrating by parts one obtains

$$\int_0^{\Delta} A(z)B'(z)\,\mathrm{d}z + \int_0^{\Delta} A'(z)B(z)\,\mathrm{d}z = A(z)B(z) \Big|_{z=0}^{z=\Delta} \tag{24}$$

As a result, substituting (23) and (24) into (21), $\mathscr{B}_2$ becomes

$$\mathscr{B}_2 = A(z)B(z) \Big|_{z=0}^{z=\Delta} \frac{r^{2\alpha+1}}{2\alpha+1} \Bigg|_{r=R^*}^{r=R} \int_0^{\omega_{12}} \mathbf{f}^{\mathrm{T}}[A_z]^{\mathrm{T}}[E](\alpha[A_r]\mathbf{f} + [A_\theta]\mathbf{f}')\,\mathrm{d}\theta \tag{25}$$

We are now in the stage where we can gather all parts that contribute to the weak formulation. Substituting (15)–(22), into (6), and noting that (25) is identical to the first part of $\mathscr{F}_1$ given in (15) one obtains

$$\left(\int_0^{\Delta} A(z)B(z)\,\mathrm{d}z \right) \int_{R^*}^{R} \int_0^{\omega_{12}} \left\{ \left([A_r]\partial_r + [A_\theta]\frac{\partial_\theta}{r} \right) \tilde{\mathbf{v}} \right\}^{\mathrm{T}} [E] \left\{ \left([A_r]\partial_r + [A_\theta]\frac{\partial_\theta}{r} \right) \tilde{\mathbf{u}} \right\} r\,\mathrm{d}\theta\,\mathrm{d}r$$
$$+ \left(\int_0^{\Delta} A'(z)B'(z)\,\mathrm{d}z \right) \int_{R^*}^{R} \int_0^{\omega_{12}} \tilde{\mathbf{v}}^{\mathrm{T}}[A_z]^{\mathrm{T}}[E][A_z]\tilde{\mathbf{u}}\,r\,\mathrm{d}r\,\mathrm{d}\theta$$
$$= \left(\int_0^{\Delta} A(z)B(z)\,\mathrm{d}z \right) \left\{ \alpha \int_0^{\omega_{12}} \tilde{\mathbf{v}}^{\mathrm{T}}[A_r]^{\mathrm{T}}[E][A_r]\tilde{\mathbf{u}} \Big|_{r=R^*}^{r=R} \mathrm{d}\theta \right.$$
$$\left. + \int_0^{\omega_{12}} \tilde{\mathbf{v}}^{\mathrm{T}}[A_r]^{\mathrm{T}}[E][A_\theta]\partial_\theta\tilde{\mathbf{u}} \Big|_{r=R^*}^{r=R} \mathrm{d}\theta \right\} +$$

$$+ A'(z)B(z)\Big|_{z=0}^{z=\Delta}\int_{R^*}^{R}\int_0^{\omega_{12}}\tilde{\mathbf{v}}^{\mathrm{T}}[A_z]^{\mathrm{T}}[E][A_z]\tilde{\mathbf{u}}\,r\,\mathrm{d}\theta\,\mathrm{d}r$$

$$+\int_0^{\Delta}A'(z)B(z)\,\mathrm{d}z\int_0^{\omega_{12}}r\tilde{\mathbf{v}}^{\mathrm{T}}[A_r]^{\mathrm{T}}[E][A_z]\tilde{\mathbf{u}}\Big|_{r=R^*}^{r=R}\mathrm{d}\theta \tag{26}$$

Rearranging (26), using integration by parts, and dividing by $\int_0^{\Delta}A(z)B(z)\,\mathrm{d}z$, (26) becomes

$$\int_{R^*}^{R}\int_0^{\omega_{12}}\left\{\left([A_r]\partial_r+[A_\theta]\frac{\partial_\theta}{r}\right)\tilde{\mathbf{v}}\right\}^{\mathrm{T}}[E]\left\{\left([A_r]\partial_r+[A_\theta]\frac{\partial_\theta}{r}\right)\tilde{\mathbf{u}}\right\}r\,\mathrm{d}\theta\,\mathrm{d}r$$

$$-\int_0^{\omega_{12}}\tilde{\mathbf{v}}^{\mathrm{T}}[A_r]^{\mathrm{T}}[E][A_\theta]\partial_\theta\tilde{\mathbf{u}}\Big|_{r=R^*}^{r=R}\mathrm{d}\theta$$

$$=\alpha\int_0^{\omega_{12}}\tilde{\mathbf{v}}^{\mathrm{T}}[A_r]^{\mathrm{T}}[E][A_r]\tilde{\mathbf{u}}\Big|_{r=R^*}^{r=R}\mathrm{d}\theta$$

$$+\frac{\displaystyle\int_0^{\Delta}A''(z)B(z)\,\mathrm{d}z}{\displaystyle\int_0^{\Delta}A(z)B(z)\,\mathrm{d}z}\int_{R^*}^{R}\int_0^{\omega_{12}}\tilde{\mathbf{v}}^{\mathrm{T}}[A_z]^{\mathrm{T}}[E][A_z]\tilde{u}\,r\,\mathrm{d}\theta\,\mathrm{d}r$$

$$+\frac{\displaystyle\int_0^{\Delta}A'(z)B(z)\,\mathrm{d}z}{\displaystyle\int_0^{\Delta}A(z)B(z)\,\mathrm{d}z}\int_0^{\omega_{12}}r\tilde{\mathbf{v}}^{\mathrm{T}}[A_r]^{\mathrm{T}}[E][A_z]\tilde{\mathbf{u}}\Big|_{r=R^*}^{r=R}\mathrm{d}\theta \tag{27}$$

The obtained formulation is an eigen-problem cast in the weak sense. However, the edge eigen pairs *are independent of the coordinate z*, i.e. are independent of the edge stress intensity factors $A(z)$ or their derivatives. Thus, the two last expressions in (27) must vanish, obtaining the *Modified Steklov* formulation for the edge eigenpairs

$$\text{Seek } \alpha\in\mathscr{C},\quad \mathbf{0}\neq\tilde{\mathbf{u}}\in[H^1(\tilde{\Omega}_R^*)]^3,\text{ such that},\quad \forall\tilde{\mathbf{v}}\in[H^1(\tilde{\Omega}_R^*)]^3$$

$$\tilde{\mathscr{B}}(\tilde{\mathbf{u}},\tilde{\mathbf{v}})-[\mathscr{N}_R(\tilde{\mathbf{u}},\tilde{\mathbf{v}})-\mathscr{N}_{R^*}(\tilde{\mathbf{u}},\tilde{\mathbf{v}})]=\alpha[\mathscr{M}_R(\tilde{\mathbf{u}},\tilde{\mathbf{v}})-\mathscr{M}_{R^*}(\tilde{\mathbf{u}},\tilde{\mathbf{v}})] \tag{28}$$

$\tilde{\Omega}_R^*$ is the two-dimensional domain which is the flat surface bounded by $0\leqslant\theta\leqslant\omega_{12}$ and $R^*\leqslant r\leqslant R$ and

$$\tilde{\mathscr{B}}(\tilde{\mathbf{u}},\tilde{\mathbf{v}})\overset{\text{def}}{=}\int_{R^*}^{R}\int_0^{\omega_{12}}\left\{\left([A_r]\partial_r+[A_\theta]\frac{\partial_\theta}{r}\right)\tilde{\mathbf{v}}\right\}^{\mathrm{T}}[E]\left\{\left([A_r]\partial_r+[A_\theta]\frac{\partial_\theta}{r}\right)\tilde{\mathbf{u}}\right\}r\,\mathrm{d}\theta\,\mathrm{d}r \tag{29}$$

$$\mathscr{N}_R(\tilde{\mathbf{u}},\tilde{\mathbf{v}})\overset{\text{def}}{=}\int_0^{\omega_{12}}\tilde{\mathbf{v}}^{\mathrm{T}}[A_r]^{\mathrm{T}}[E][A_\theta]\partial_\theta\tilde{\mathbf{u}}\Big|_{r=R}\mathrm{d}\theta \tag{30}$$

$$\mathscr{M}_R(\tilde{\mathbf{u}},\tilde{\mathbf{v}})\overset{\text{def}}{=}\int_0^{\omega_{12}}\tilde{\mathbf{v}}^{\mathrm{T}}[A_r]^{\mathrm{T}}[E][A_r]\tilde{\mathbf{u}}\Big|_{r=R}\mathrm{d}\theta \tag{31}$$

Remark 1. Although the test and trial functions have three components, the domain over which the weak eigenformulation is defined is two-dimensional, and excludes any singular points. Therefore the application of the *p*-version of the FEM for solving (28) is expected to be very efficient.

Remark 2. The bilinar forms $\mathscr{N}_R$ and $\mathscr{N}_{R^*}$ are *non-symmetric* with respect to $\tilde{\mathbf{u}}$ and $\tilde{\mathbf{v}}$, thus the problem formulated in the weak sense loses its self-adjoint property. As a consequence, the 'minimax principle' does not hold, therefore the approximated eigenvalues (obtained by a series of hierarchical family of trial functions) cannot be considered as an upper bound of the exact ones and the monotonic behaviour of the error is lost as well. Nevertheless, convergence is assured (with a very high rate as will be shown by the numerical examples) under a general proof provided in Reference 22.

Remark 3. Note that the weak eigenformulation (28) is not limiting the domain $\tilde{\Omega}_R^*$ to be isotropic, and in fact (28) can be applied to multi-material anisotropic interface, as will be demonstrated by numerical examples.

3. NUMERICAL TREATMENT BY THE FINITE ELEMENT METHOD

In the following, the weak eigenformulation (28) is discretized by considering a finite dimensional sub-space of $[H^1(\tilde{\Omega}_R^*)]^3$, employing the *p*-version of the finite element method.

Assume that the domain $\tilde{\Omega}_R^*$ consists of three different materials as shown in Figure 4. We divided $\tilde{\Omega}_R^*$ into, let us say 3 finite elements, through a meshing process. Let us consider a typical element, element number 1, shown in Figure 4, bounded by $\theta_1 \leqslant \theta \leqslant \theta_2$. A standard element in the ξ, η plane such that $-1 < \xi < 1$, $-1 < \eta < 1$ is considered, over which the polynomial basis and trial functions are defined. These standard elements are then mapped by appropriate mapping functions onto the 'real' elements (for details see Reference 21, Chapters, 5, 6). The functions $\tilde{u}_x$, $\tilde{u}_y$, $\tilde{u}_z$ are expressed in terms of the basis functions $\Phi_i(\xi, \eta)$ in the

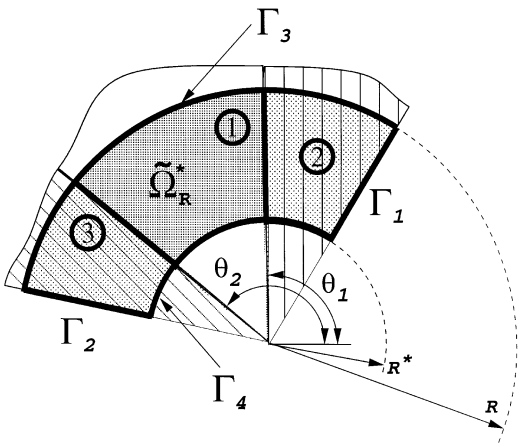

Figure 4. A typical finite element mesh in the domain $\tilde{\Omega}_R^*$

standard plane:

$$\left.\begin{aligned}\tilde{u}_x(\xi,\eta) &= \sum_{i=1}^{N} a_i \Phi_i(\xi,\eta)\\ \tilde{u}_y(\xi,\eta) &= \sum_{i=1}^{N} a_{N+i} \Phi_i(\xi,\eta)\\ \tilde{u}_z(\xi,\eta) &= \sum_{i=1}^{N} a_{2N+i} \Phi_i(\xi,\eta)\end{aligned}\right\} \tag{32}$$

or

$$\tilde{\mathbf{u}} = \begin{bmatrix} \Phi_1 \ldots \Phi_N & 0 \ldots 0 & 0 \ldots 0 \\ 0 \ldots 0 & \Phi_1 \ldots \Phi_N & 0 \ldots 0 \\ 0 \ldots 0 & 0 \ldots 0 & \Phi_1 \ldots \Phi_N \end{bmatrix} \begin{Bmatrix} a_1 \\ \vdots \\ a_{3N} \end{Bmatrix} \stackrel{\text{def}}{=} [\Phi]\mathbf{a} \tag{33}$$

where a_i are the amplitudes of the basis functions, and Φ_i are products of integrals of Legendre polynomials in ξ and η. $\tilde{\mathbf{u}}$ and $\tilde{\mathbf{v}}$ lie in the same space, therefore, we define similarly $\tilde{\mathbf{v}} \stackrel{\text{def}}{=} [\Phi]\mathbf{b}$.

Using (33) the unconstrained stiffness matrix corresponding to $\tilde{\mathscr{B}}(\tilde{\mathbf{u}}, \tilde{\mathbf{v}})$ on the typical element is given by

$$[K] \stackrel{\text{def}}{=} \int_{R^*}^{R} \int_{\theta_1}^{\theta_2} \left\{ \left([A_r]\partial_r + [A_\theta] \frac{\partial_\theta}{r} \right) [\Phi] \right\}^{\mathrm{T}} [E] \left\{ \left([A_r]\partial_r + [A_\theta] \frac{\partial_\theta}{r} \right) [\Phi] \right\} r \, \mathrm{d}\theta \, \mathrm{d}r \tag{34}$$

We concentrate our discussion now on $\mathscr{N}(\tilde{\mathbf{u}}, \tilde{\mathbf{v}})$. We start by evaluating the required expressions involved in the computation. The mapping of ξ, $\eta = -1$ (side 1 of the standard element) onto Γ_3 is given by the following:

$$\theta = \frac{\theta_2 - \theta_1}{2} \xi + \frac{\theta_2 + \theta_1}{2} \tag{35}$$

so that $\mathrm{d}\theta = \frac{1}{2}(\theta_2 - \theta_1)\,\mathrm{d}\xi$, and the expression $[A_\theta]\partial_\theta \tilde{\mathbf{u}}\,\mathrm{d}\theta$ becomes

$$[A_\theta]\partial_\theta \tilde{\mathbf{u}}\,\mathrm{d}\theta = [A_\theta]\partial_\xi \tilde{\mathbf{u}}\,\mathrm{d}\xi \tag{36}$$

On side 1 the basis and trial functions $\Phi_i(\xi, \eta = -1)$ are nothing more than integrals of Legendre polynomials $P_i(\xi)$ for $i > 3$, and $P_1(\xi) = (1 - \xi)/2$, $P_2(\xi) = (1 + \xi)/2$ (see, for details, Reference 21, Chapters 3, 6). By defining the following matrix:

$$[\partial P] \stackrel{\text{def}}{=} \begin{bmatrix} -P_1' \sin\theta & \ldots & -P_N' \sin\theta & 0 & \ldots & 0 & 0 & \ldots & 0 \\ 0 & \ldots & 0 & P_1' \cos\theta & \ldots & P_N' \cos\theta & 0 & \ldots & 0 \\ 0 & \ldots & 0 & 0 & \ldots & 0 & 0 & \ldots & 0 \\ P_1' \cos\theta & \ldots & P_N' \cos\theta & -P_1' \sin\theta & \ldots & -P_N' \sin 0 & 0 & \ldots & 0 \\ 0 & \ldots & 0 & 0 & \ldots & 0 & P_1' \cos\theta & \ldots & P_N' \cos\theta \\ 0 & \ldots & 0 & 0 & \ldots & 0 & -P_1' \sin\theta & \ldots & -P_N' \sin\theta \end{bmatrix}$$

(36) becomes

$$[A_\theta]\partial_\xi \tilde{\mathbf{u}}\, \mathrm{d}\xi = [\partial P]\mathbf{a}\, \mathrm{d}\xi \tag{37}$$

We also define the matrix

$$[\tilde{P}] \overset{\text{def}}{=} \begin{bmatrix} P_1\cos\theta & \dots & P_N\cos\theta & 0 & \dots & 0 & 0 & \dots & 0 \\ 0 & \dots & 0 & P_1\sin\theta & \dots & P_N\sin\theta & 0 & \dots & 0 \\ 0 & \dots & 0 & 0 & \dots & 0 & 0 & \dots & 0 \\ P_1\sin\theta & \dots & P_N\sin\theta & P_1\cos\theta & \dots & P_N\cos\theta & 0 & \dots & 0 \\ 0 & \dots & 0 & 0 & \dots & 0 & P_1\sin\theta & \dots & P_N\sin\theta \\ 0 & \dots & 0 & 0 & \dots & 0 & P_1\cos\theta & \dots & P_N\cos\theta \end{bmatrix}$$

so that the expression $\tilde{\mathbf{v}}^{\mathrm{T}}[A_r]^{\mathrm{T}}$ becomes

$$\tilde{\mathbf{v}}^{\mathrm{T}}[A_r]^{\mathrm{T}} = \mathbf{b}^{\mathrm{T}}[\tilde{P}]^{\mathrm{T}} \tag{38}$$

Substituting (37) and (38) into (30) we obtain the expression for $\mathscr{N}_R(\tilde{u}, \tilde{v})$

$$\mathscr{N}_R(\tilde{\mathbf{u}}, \tilde{\mathbf{v}}) = b^{\mathrm{T}}\left(\int_{-1}^{1} [\tilde{P}]^{\mathrm{T}}[E][\partial P]\Big|_{\eta=-1} \mathrm{d}\xi\right)\mathbf{a} \overset{\text{def}}{=} \mathbf{b}^{\mathrm{T}}[N_R]\mathbf{a} \tag{39}$$

The entries of $[N_R]$ are computed using the Gauss quadrature

$$(N_R)_{ij} = \sum_{m=1}^{M} W_m \sum_{l,k=1}^{6} \tilde{P}_{li}(\xi_m) E_{lk} \partial P_{kj}(\xi_m) \tag{40}$$

where W_m and ξ_m are the weights and abscissas of the Gauss quadrature points, respectively.

Using the same arguments as above, the expression $\mathscr{M}_R(\tilde{\mathbf{u}}, \tilde{\mathbf{v}})$ in (31) is evaluated

$$\mathscr{M}_R(\tilde{\mathbf{u}}, \tilde{\mathbf{v}}) = \mathbf{b}^{\mathrm{T}}\left(\frac{\theta_2 - \theta_1}{2}\int_{-1}^{1} [\tilde{P}]^{\mathrm{T}}[E][\tilde{P}]\Big|_{\eta=-1} \mathrm{d}\xi\right)\mathbf{a} \overset{\text{def}}{=} \mathbf{b}^{\mathrm{T}}[M_R]\mathbf{a} \tag{41}$$

and

$$(M_R)_{ij} = \frac{\theta_2 - \theta_1}{2} \sum_{m=1}^{M} W_m \sum_{l,k=1}^{6} \tilde{P}_{li}(\xi_m) E_{lk} \tilde{P}_{kj}(\xi_m) \tag{42}$$

The matrices $[N_{R^*}]$ and $[M_{R^*}]$ have same values as those of $[N_R]$ and $[M_R]$, but of opposite sign. This is because the shape functions on the artifical boundaries Γ_3 and Γ_4 are the same (except for some sign changes), and so is the mapping to the standard plane. Denoting the set of amplitudes of the basis functions associated with the artificial boundary Γ_3 by $\mathbf{a}_R$, and those associated with the artificial boundary Γ_4 by $\mathbf{a}_{R^*}$, the eigenpairs can be obtained by solving the generalized matrix eigen problem:

$$[K]\mathbf{a} - ([N_R]\mathbf{a}_R - [N_{R^*}]\mathbf{a}_{R^*}) = \alpha([M_R]\mathbf{a}_R - [M_{R^*}]\mathbf{a}_{R^*}) \tag{43}$$

Augmenting the coefficients of the basis functions associated with Γ_3 with those associated with Γ_4, and denoting them by the vector $\mathbf{a}_{RR^*}$, (43) becomes

$$[K]\mathbf{a} - [N_{RR^*}]\mathbf{a}_{RR^*} = \alpha[M_{RR^*}]\mathbf{a}_{RR^*} \tag{44}$$

We assemble the left-hand side of (44). The vector which represents the total number of nodal values in $\tilde{\Omega}_R^*$ may be divided into two vectors such that one contains the coefficients $\mathbf{a}_{RR^*}$, and the other contains the remaining coefficients: $\mathbf{a}^{\mathrm{T}} = \{\mathbf{a}_{RR^*}^{\mathrm{T}}, \mathbf{a}_{\mathrm{in}}^{\mathrm{T}}\}$. By partitioning $[K]$, we can write the eigenproblem (44) in the form

$$\begin{bmatrix} [K_{RR^*}] - [N_{RR^*}] & [K_{RR^*-\mathrm{in}}] \\ [K_{\mathrm{in}-RR^*}] & [K_{\mathrm{in}}] \end{bmatrix} \begin{Bmatrix} \mathbf{a}_{RR^*} \\ \mathbf{a}_{\mathrm{in}} \end{Bmatrix} = \alpha \begin{bmatrix} [M_{RR^*}] & [0] \\ [0] & [0] \end{bmatrix} \begin{Bmatrix} \mathbf{a}_{RR^*} \\ \mathbf{a}_{\mathrm{in}} \end{Bmatrix} \tag{45}$$

The relation in (45) can be used to eliminate $\mathbf{a}_{\mathrm{in}}$ by static condensation, thus obtaining the reduced eigenproblem

$$[K_S]\mathbf{a}_{RR^*} = \alpha[M_{RR^*}]\mathbf{a}_{RR^*} \tag{46}$$

where

$$[K_S] = ([K_{RR^*}] - [N_{RR^*}]) - [K_{RR^*-\mathrm{in}}][K_{\mathrm{in}}]^{-1}[K_{\mathrm{in}-RR^*}]$$

It is possible to eliminate the unknowns $\mathbf{a}_{\mathrm{in}}$ from the matrix $[K]$, because the relevant equations do not involve the as yet unknown eigenvalues α.

For the solution of the eigenproblem (46), it is important to note that $[K_S]$ is, in general, a full matrix. However, since the order of the matrices is relatively small, the solution (using Cholesky factorization to compute $[K_{\mathrm{in}}]^{-1}$) is not expensive. Details on the implementation issues for solving the generalized eigenvalue problem can be found in Reference 23.

Remark 4. There is the possibility that an eigenvalue is repeated m times with less than m corresponding eigenvectors (the algebraic multiplicity is higher than the geometric multiplicity). This is associated with the special cases when the asymptotic expansion contains logarithmic terms, and this behavior triggers the existence of $\ln(r)$ terms.

Remark 5. Although we derived our matrices as if only one finite element exists along the boundary Γ_3 and Γ_4, the formulation for multiple finite elements is identical, and the matrices $[K]$, $[N_R]$ and $[M_R]$ are obtained by an assembly procedure.

4. NUMERICAL INVESTIGATION

The performance of the modified Steklov weak formulation is demonstrated in the following subsections on several test cases for which the exact eigenvalues are known. We first consider a plane crack in an isotropic material, and at the interface of a bi-material interface, followed by the computation of eigenpairs associated with free edge effects in two cross-ply anisotropic laminate. These three examples demonstrate the robustness, efficiency and accuracy of the proposed numerical methods for extracting eigenpairs.

4.1. Plane crack in isotropic domains

Consider a plane crack in an isotropic material as shown in Figure 5. The material properties are $E = 1$ and $\nu = 0{\cdot}3$. The exact first three eigenpairs for this example problem are

$\alpha_1 = \alpha_2 = \alpha_3 = 0{\cdot}5$, and in linear elastic fracture mechanics terminology they are associated with deformation modes I, II and III. This example problem has been used to demonstrate the accuracy which is typically achieved with the proposed numerical method.

A four-element mesh has been used as shown in Figure 6, and over each element the polynomial degree of the shape functions has been increased from 1 to 8. In all examples $R = 1$. As will be shown in the following the magnitude of R^* has virtually no influence on the accuracy of the obtained eigenpairs, and as $R^* \to 1$ the accuracy of the results slightly improves, therefore the value $R^* = 0{\cdot}99$ is used in all computations. The relative error (%) in the ith eigenvalue is defined by

$$e_{\alpha_i}(\%) = 100\,\frac{\alpha_i^{\mathrm{FE}} - \alpha_i}{\alpha_i} \tag{47}$$

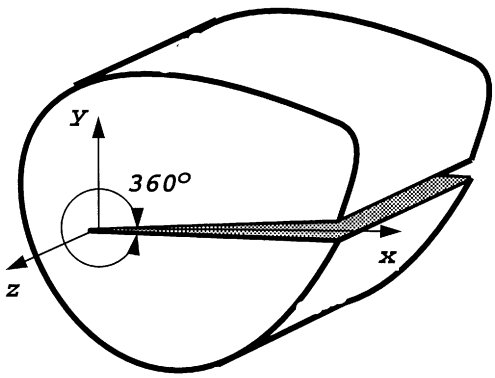

Figure 5. A typical plane crack in isotropic domains

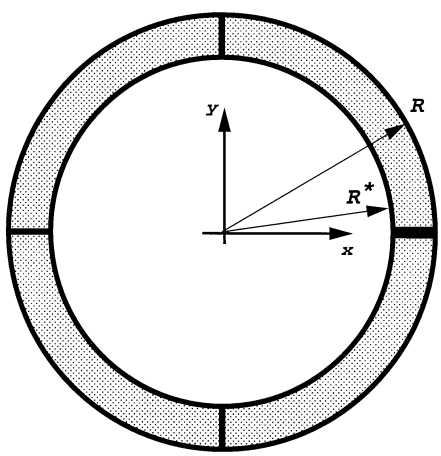

Figure 6. Finite element mesh used for the plane crack in isotropic domain

We summarize the relative error (%) in the first 3 eigenvalues, the number of degrees of freedom before performing static condensation, and the CPU elapsed time† required for the computation in Table I. The rate of convergence of the eigenvalues (reported in Table I) is clearly visible when plotted on a log–log scale as shown in Figure 7. This shows the rapid but non-monotonic convergence rate as expected. To demonstrate the influence of R^* on the obtained results, Figure 8 presents the absolute relative error (%) in the first three eigenvalues at $p = 8$ *as* R^* varies from 0·5 to 0·99.

4.2. *Plane crack at bi-material interface*

Consider a bi-material interface which is composed of two homogeneous materials, with continuity of tractions and displacements across interface maintained. The two materials are

Table I. Relative error (%) in the first 3 eigenvalues—Plane crack edge in isotropic domain

p-level	$p=1$	$p=2$	$p=3$	$p=4$	$p=5$	$p=6$	$p=7$	$p=8$
DOF	30	69	108	159	222	297	384	483
CPU (s)	0·17	0·48	2·4	2·2	3·9	6·4	10·8	16·4
e-val #								
e_{α_1}	0·06	− 0·199	− 0·004	− 0·00007	− 0·0000030	0·0000011	− 0·000000019	− 0·000000039
e_{α_2}	1·97	− 0·0977	− 0·00078	− 0·000016	0·0000021	− 0·00000057	− 0·000000031	0·000000032
e_{α_3}	2·57	0·0256	0·0001	0·00000028	− 0·0000000015	0·0000000097	0·000000005	− 0·00000000035

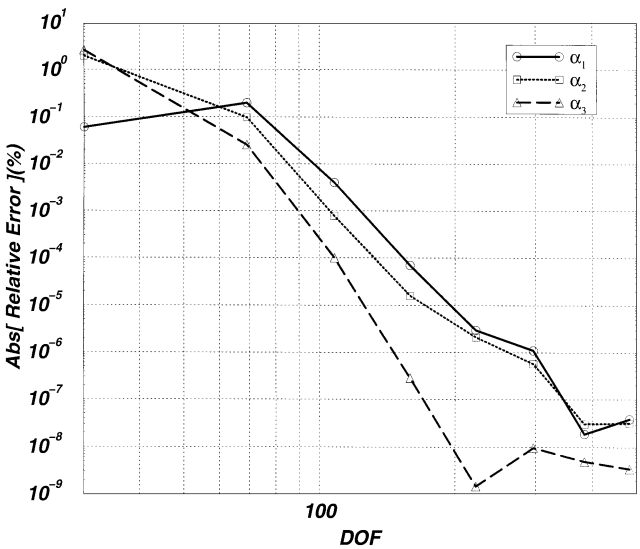

Figure 7. Convergence of approximated eigenvalues for plane crack edge in isotropic domain

† Computations performed on a SGI Indigo^2 machine, with a R4400 200 MHz processor, Specfp92 = 131

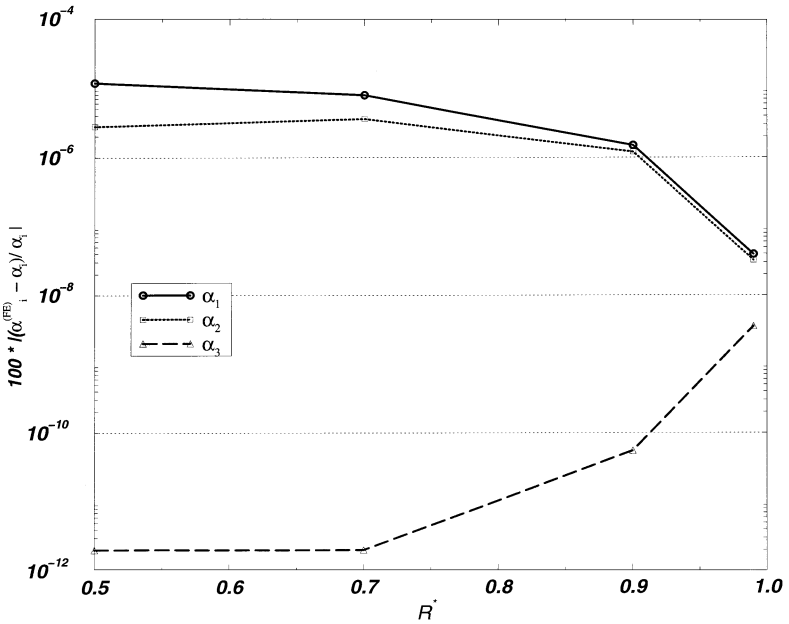

Figure 8. R^* influence on eigenvalues accuracy (plane crack edge in isotropic domain)

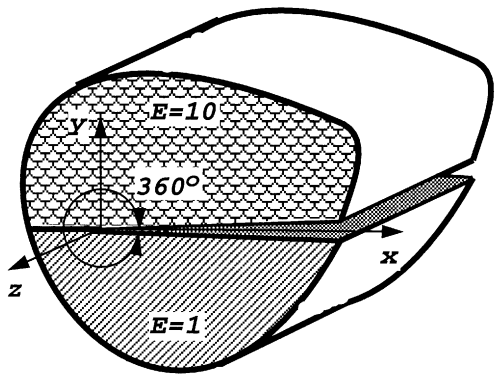

Figure 9. Plane crack at bi-material interface

isotropic, both having Poisson ratio 0·3, the upper material having $E = 10$ and the lower $E = 1$. We are interested in plane cracks at the interface of the two materials as shown in Figure 9. This example problem has been chosen to demonstrate the method's performance for cases where complex eigenpairs arise. The exact first three eigenpairs for this example problem are $\alpha_{1,2} = 0{\cdot}5 \pm i0{\cdot}07581177769$ and $\alpha_3 = 0{\cdot}5$. In linear elastic fracture mechanics terminology α_1 and α_2 are associated with deformation in the x–y plane (where mode I and mode II are coupled in this case), and α_3 is the out-of-plane mode.

The same four-element mesh as shown in Figure 6 has been used for the computations. The relative error (%) in the first two eigenvalues is split in two: one defining the relative error in the real part and being denoted by $e_{\mathscr{R}\alpha_{1,2}}$ and the other defining the relative error in the imaginary part $e_{\mathscr{I}\mathrm{m}\alpha_{1,2}}$

$$e_{\mathscr{R}\alpha_{1,2}}(\%) = 100\,\frac{\mathscr{R}\alpha_1^{\mathrm{FE}} - \mathscr{R}\alpha_1}{\mathscr{R}\alpha_1}, \quad e_{\mathscr{I}\mathrm{m}\alpha_{1,2}}(\%) = 100\,\frac{\mathscr{I}\mathrm{m}\alpha_1^{\mathrm{FE}} - \mathscr{I}\mathrm{m}\alpha_1}{\mathscr{I}\mathrm{m}\alpha_1} \tag{48}$$

Since we are using exactly the same mesh as in the previous example problem, the number of degrees of freedom and the CPU elapsed time for computations remain as reported in Table I. We summarize the relative error (%) in the first 3 eigenvalues in Table II. The method provides excellent results for complex eigenpairs as well, with no deterioration in the performance.

4.3. *Two cross-ply anisotropic laminate*

We study edge singularities associated with a two cross-ply anisotropic laminate. Consider a composite laminate with ply properties typical of a high modulus graphite–epoxy system, as

Table II. Relative error (%) in the first eigenvalues—plane crack edge at bi-material interface

p-level	$p=1$	$p=2$	$p=3$	$p=4$	$p=5$	$p=6$	$p=7$	$p=8$
e-val #								
$e_{\mathscr{R}\alpha_{1,2}}$	1·03	− 0·196	− 0·011	− 0·00050	− 0·000014	5·2e − 11	− 0·0000000028	− 0·0000000025
$e_{\mathscr{I}\mathrm{m}\alpha_{1,2}}$	− 95	− 15·5	− 1·118	− 0·0425	0·0010	− 0·000017	0·000000013	0·000000079
e_{α_3}	2·59	0·0256	0·0001	0·00000028	− 0·0000000015	0·0000000097	0·000000005	− 0·0000000035

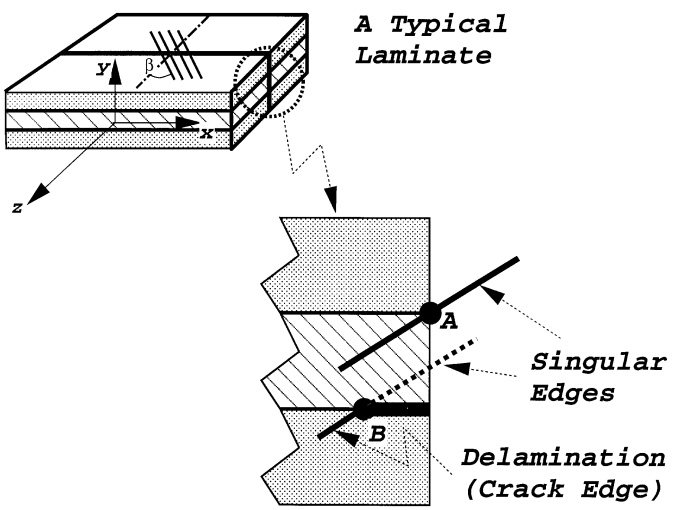

Figure 10. Cross-ply anisotropic laminate

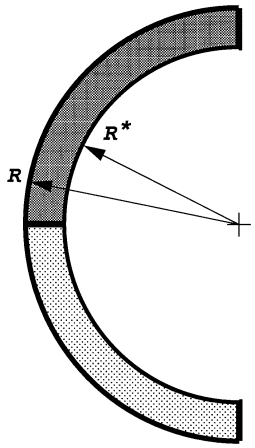

Figure 11. Finite element mesh used for the cross-ply anisotropic laminate

Table III. Relative error (%) in the first 5 non-integer eigenvalues—Cross-ply anisotropic laminate

p-level	$p=1$	$p=2$	$p=3$	$p=4$	$p=5$	$p=6$	$p=7$	$p=8$
DOF	18	39	60	87	120	159	204	255
CPU (s)	0·12	0·23	0·48	0·92	1·54	2·41	4·19	6·08
e-val #								
e_{α_1}	− 7·5	− 0·44	− 0·38	0·056	− 0·018	− 0·0067	− 0·000825	− 0·00006
$e_{\Re\alpha_{2,3}}$	− 30·4	− 15·21	− 0·298	− 0·228	− 0·053	− 0·0064	− 0·0022	− 0·00033
$e_{\Im\mathrm{m}\alpha_{2,3}}$	**	**	− 15·71	− 3·196	0·112	0·106	0·0077	− 0·00004
$e_{\Re\alpha_{4,5}}$	− 7·75	6·11	4·05	0·315	− 0·187	− 0·122	− 0·013	− 0·0034
$e_{\Im\mathrm{m}\alpha_{4,5}}$	**	**	− 18·52	− 11·43	− 1·13	− 0·041	0·073	0·0135

** No imaginary part

shown in Figure 10. The orientation of fibres differs from layer to layer. Referring to the principle direction of the fibres, we define

$$E_L = 20\times 10^6 \text{ psi} \quad E_T = E_z = 2.1\times 10^6 \text{ psi}$$

$$G_{LT} = G_{Lz} = G_{Tz} = 0{\cdot}85\times 10^6 \text{ psi} \quad v_{LT} = v_{Lz} = v_{Tz} = 0{\cdot}21$$

where the subscripts L, T, z refer to fibre, transverse and thickness directions of an individual ply, respectively. The material matrix $[E]$ for a ply with fibres orientation rotated by an angle β about the y-axis is given by

$$[E] = [T(\beta)]^{\mathrm{T}}[E_0][T(\beta)]$$

where

$$[T(\beta)] = \begin{pmatrix} s^2 & 0 & c^2 & 0 & 0 & c\cdot s \\ 0 & 1 & 0 & 0 & 0 & 0 \\ c^2 & 0 & s^2 & 0 & 0 & -c\cdot s \\ 0 & 0 & 0 & s & c & 0 \\ 0 & 0 & 0 & -c & s & 0 \\ -2c\cdot s & 0 & 2c\cdot s & 0 & 0 & s^2-c^2 \end{pmatrix}, \quad c \overset{\text{def}}{=} \cos(\beta), \quad s \overset{\text{def}}{=} \sin(\beta)$$

$$[E_0] = V \begin{pmatrix} (1-v_{Tz}v_{zT})E_L & (v_{LT}+v_{Lz}v_{zT})E_T & (v_{zL}+v_{zT}v_{TL})E_L & 0 & 0 & 0 \\ & (1-v_{Lz}v_{zL})E_L & (v_{zT}+v_{LT}v_{zL})E_T & 0 & 0 & 0 \\ & & (1-v_{LT}v_{TL})E_z & 0 & 0 & 0 \\ & & & \dfrac{G_{Tz}}{V} & 0 & 0 \\ & & & & \dfrac{G_{Lz}}{V} & 0 \\ & & & & & \dfrac{G_{LT}}{V} \end{pmatrix}$$

$$V \overset{\text{def}}{=} (1 - v_{LT}v_{TL} - v_{Tz}v_{zT} - v_{Lz}v_{zL} - 2v_{LT}v_{Tz}v_{zL})^{-1}$$

$$v_{TL} = v_{LT}\frac{E_T}{E_L}, \quad v_{zT} = v_{Tz}\frac{E_z}{E_T}, \quad v_{zL} = v_{Lz}\frac{E_z}{E_L}$$

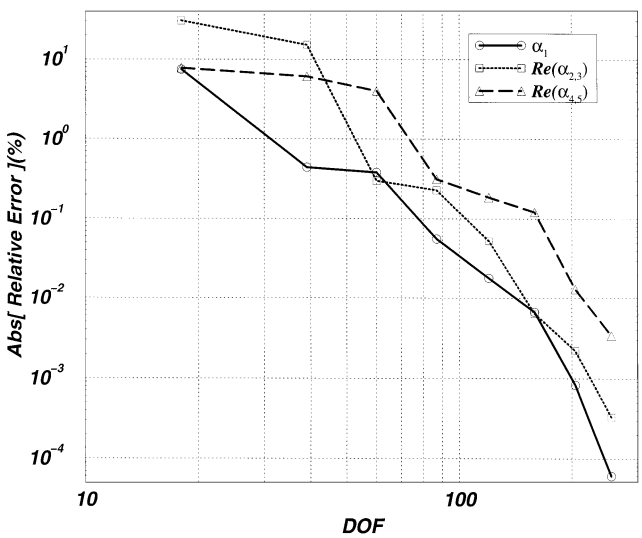

Figure 12. Convergence of approximated eigenvalues for the cross-ply anisotropic laminate

We first investigate the eigenpairs associated with the singularities near the junction of the free edge and the interface, *edge A* in Figure 10, for a commonly used $[\pm\beta]$ angle-ply composite. Of course, the eigenpairs depend on β and we chose $\beta = 45^\circ$ for which the first 12 exact non-integer eigenpairs are reported in [15] with 8 decimal significant digits: $\alpha_1 = 0{\cdot}974424342$, $\alpha_{2,3} = 1{\cdot}88147184 \pm i0{\cdot}23400947$, $\alpha_{4,5} = 2{\cdot}5115263 \pm i0{\cdot}79281732, \ldots$.

We use in our computation the two-element mesh shown in Figure 11. We summarize the relative error (%) in the first 5 non-integer eigenvalues, the number of degrees of freedom before performing static condensation, and the CPU elapsed time required for the computation in Table III. The rate of convergence of the eigenvalues (reported in Table III) is clearly visible when plotted on a log–log scale as shown in Figure 12. Again one obtains a rapid convergence rate. The three-dimensional eigenfunctions (displacement fields) associated with α_1 obtained at $p = 8$ are illustrated in Figure 13.

The variation of the eigenvalues for different $[\pm\beta]$ cross-ply laminate is investigated in the following. We use the same mesh presented in Figure 11, with different material properties which reflect a laminate with fibers rotated at an angle $\pm\beta$ about the y-axis. The obtained eigen values reported in Table IV are accurate up to the 5 decimal digit shown. This accuracy is guaranteed because these digits have not been changed while increasing the polynomial level over the finite element mesh.

Delamination. Once a crack starts propagating between two lamina, the behaviour of the singular stress tensor changes dramatically, and the eigenpairs are different. We consider a plane-crack with a tip at the edge denoted by *edge B* in Figure 10. Again we consider a $[\pm 45^\circ]$ cross-ply

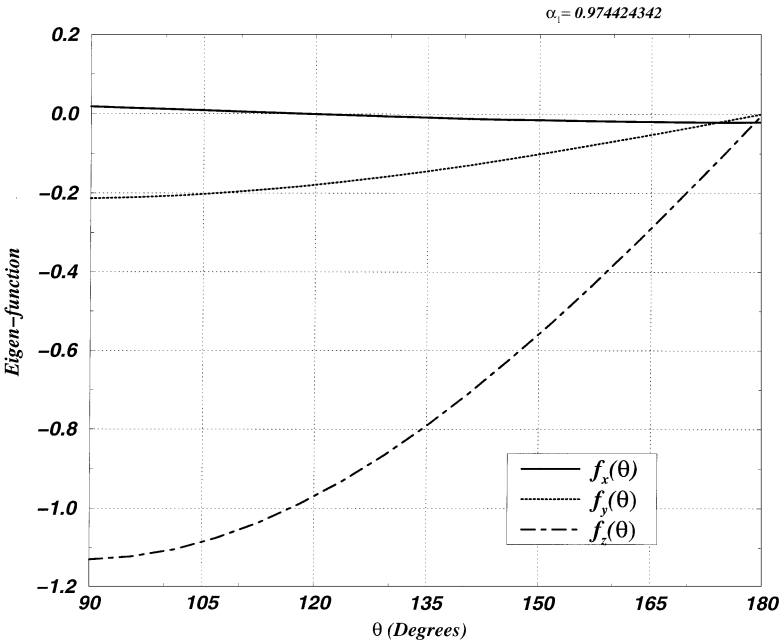

Figure 13. Eigenfunctions associated with α_1 for the cross-ply anisotropic laminate

Table IV. Eigenvalues for different $[\pm\beta]$ fibre orientation cross-ply laminate

$[\pm\beta]$	15°	30°	45°	60°	75°
α_1	0·99936	0·98834	0·97442	0·97665	0·99105

Table V. First 3 eigen-values for a crack between two laminas in a cross-ply anisotropic laminate

p-level DOF	$p=1$ 30	$p=2$ 69	$p=3$ 108	$p=4$ 159	$p=5$ 222	$p=6$ 297	$p=7$ 384	$p=8$ 483
$\mathscr{R}\alpha_{1,2}^{FE}$	0·517095	0·498988	0·500189	0·4999305	0·499995	0·500005	0·500002	0·500000
$\mathscr{I}\mathrm{m}\alpha_{1,2}^{FE}*100$	3·472695	3·464185	3·518766	3·467100	3·444288	3·437041	3·435015	3·434454
α_3^{FE}	0·516157	0·510878	0·499144	0·499133	0·499847	0·500039	0·500020	0·500001

laminate, and use a four-element mesh (as the one in Figure 6) for the computations. The first three eigenvalues and the number of DOFs at each p-level are summarized in Table V. Observing the obtained results we may conclude with a high degree of confidence that $\alpha_{1,2} = 0{\cdot}500000 \pm i0{\cdot}0343$ and $\alpha_3 = 0{\cdot}50000$.

5. SUMMARY AND CONCLUSION

We have described a numerical method, based on the modified Steklov formulation, for the reliable computation of eigenpairs resulting from three-dimensional edge singularities due to reentrant-corners, abrupt changes in material properties or boundary conditions. The formulation has been solved by means of the p-version of the finite element method, and is suitable for implementation in finite element programs. Numerical experiments for isotropic as well as anisotropic multi-material interfaces indicate that the computed values converge strongly, are accurate and inexpensive from the points of view of human time needed for input data preparation, and required CPU time. As demonstrated, the convergence behaviour is non-monotonic, however, using p-extensions excellent convergence rates were obtained.

The modified Steklov method also provides eigenpairs corresponding to infinite strain energy (i.e. $\alpha_i < 0$), which may be required for extracting stress intensity functions by the dual singular method. This is achieved because the singular point is excluded from the solution domain. This also allows a smaller domain to be analyzed and higher efficiency, due to the fact that radial refinements towards the singular edge are not required.

Although not demonstrated, the robustness of the method is maintained also when power-logarithmic stress singularities arise: the two computed distinct but adjacent eigenvalues and their corresponding eigenfunctions collapse into one as the number of degrees of freedom is increased, indicating the presence of these kind of singularities.

Computations of edge eigenpairs is important because they provides a rigorous quantitative basis for investigating failure events, such as delamination of composite materials, and failure in electronic devices. Having obtained the eigenpairs, a research project is underway for computing

the 'edge stress intensity functions' by the complementary energy principle, as described in Reference 24 in a two-dimensional setting.

REFERENCES

1. Z. Yosibash and B. A. Szabó, 'Numerical analysis of singularities in two-dimensions. Part 1: computation of eigenpairs', *Int. J. Numer. Meth. Engng*., **38,** 2055–2082 (1995).
2. M. L. Williams, 'Stress singularities resulting from various boundary conditions inangular corners of plates in extension', *Trans. ASME J. Appl. Mech*., **19,** 526–528 (1952).
3. D. B. Bogy and K. C. Wang, 'Stress singularities at interface corners in bounded dissimilar isotropic elastic materials', *Int. J. Solids Struct*., **7,** 993–1005 (1971).
4. V. L. Hein and F. Erdogan, 'Stress singularities in a two-material wedge', *Int. J. Fracture*, **7,** 317–330 (1971).
5. J. P. Dempsey and G. B. Sinclair, 'On the stress singularities in the plane elasticity of the composite edge', *J. Elasticity*, **9,** 373–391 (1979).
6. J. P. Dempsey and G. B. Sinclair, 'On the singular behavior at the vertex of a bi-material wedge', *J. Elasticity*, **11,** 317–327 (1981).
7. X. Ying, 'A reliable root solver for automatic computation with application to stress analysis of a composite plane wedige', *Ph.D. Thesis*, Washington University, St. Louis, Missouri, USA, 1986.
8. T. C. T. Ting, 'Explicit solution and invariance of the singularities at an interface crack in anisotropic composities', *Int. J. Solids Struct*., **22,** 965–983 (1986).
9. D. Leguillon and E. Sanchez-Palencia, *Computation of Singular Solutions in Elliptic Problems and Elasticity*, Wiley, New York, NY, 1987.
10. R. Barsoum, 'Theoretical basis of the finite element iterative method for the eigenvalue problem in stationary cracks', *Int. J. Numer. Meth. Engng*., **26,** 531–539 (1988).
11. M. Costabel and M. Dauge, 'Computation of corner singularities in linear elasticity', in M. Costabel, M. Dauge and S. Nicaise (eds.), *Boundary Value Problems and Integral Equations in Nonsmooth Domains*, Marcel Dekker, New York, 1995, pp. 59–68.
12. L. Gu and T. Belytschko, 'A numerical study of stress singularities in a two-material wedge', *Int. J. Solids Struct*., **31,** 865–889 (1994).
13. P. Papadakis and I. Babuška, 'A numerical procedure for the determination of certain quantities related to stress intensity factors in two-dimensional elasticity', *Comput. Methods Appl. Mech. Engng*., **122,** 69–92 (1995).
14. S. S. Pageau, P. F. Joseph and S. B. Jr. Biggers, 'Finite element analysis of anisotropic materials with singular inplane stress fields', *Int. J. Solids Struct*., **32,** 571–591 (1995).
15. S. S. Wang and I. Choi, 'Boundary layer effects in composite laminates: Part 1—free edge stress singularities', *Trans. ASME J. Appl. Mech*., **49,** 541–548 (1982).
16. S. S. Pageau and S. B. Jr. Biggers, 'A finite element approach to three dimensional singular stress states in anisotropic multi-material wedges and junctions', *Int. J. Solids Struct*., **33,** 33–47 (1996).
17. M. Dauge, *Elliptic Boundary Value Problems in Corner Domains—Smoothness and Asymptotics of Solutions*, Lecture Notes in Mathematics vol. 1341, Springer, Heidelberg, 1988.
18. P. Grisvard, *Singularities in Boundary Value Problems*, Masson, France, 1992.
19. S. Nicaise and A.-M. Sändig, 'General interface problems I & II', *Math. Methods Appl. Sci.* **17,** 395–450 (1994).
20. B. Andersson, U. Falk, I. Babuška and T. Von-Petersdorff, 'Reliable stress and fracture mechanics analysis of complex components using a h-p version of FEM', *Int. J. Numer. Meth. Engng*., **38,** 2135–2163 (1995).
21. B. A. Szabó and I. Babuška, *Finite Element Analysis*, Wiley, New York, 1991.
22. I. Babuška and A. K. Aziz, 'Survey lectures on the mathematical foundations of finite element method', in A. K. Aziz (ed.), *The Mathematical Foundations of the Finite Element Method with Applications to Partial Differential Equations*, Academic Press, New York, NY, 1972, pp. 3–343.
23. Z. Yosibash, 'Numerical analysis of singularities and first derivatives for elliptic boundary value problems in two-dimensions', *D.Sc. Thesis*, Sever Institute of Technology, Washington University, St. Louis, Missouri, USA, 1994.
24. B. A. Szabó and Z. Yosibash, 'Numerical analysis of singularities in two-dimensions. Part 2: Computation of the generalized flux/stress intensity factors', *Int. J. Numer. Meth. Engng*., **39,** 409–434 (1996).

